Electronic and magnetic interfacial states of Ag in an $Ni_{81}Fe_{19}$ /Ag coupled multilayer

2008 J. Phys.: Condens. Matter 20 095005

(http://iopscience.iop.org/0953-8984/20/9/095005)

J. Phys.: Condens. Matter **20** (2008) 095005 (8pp) doi:10.1088/0953-8984/20/9/095005

Electronic and magnetic interfacial states of Ag in an $Ni_{81}Fe_{19}$/Ag coupled multilayer

N Jaouen[1,2], F Wilhelm[1], A Rogalev[1], J Goulon[1], L Ortega[3], J M Tonnerre[3] and A Yaresko[4]

[1] European Synchrotron Radiation Facility, BP 220, F-38043 Grenoble Cédex, France
[2] Synchrotron SOLEIL, St-Aubin, F-91192 Gif/Yvette, France
[3] Institut NEEL, CNRS and Université Joseph Fourier, BP 166, 38042 Grenoble Cedex, France
[4] Max-Planck Institute for the Chemical Physics of Solid, Dresden, Germany

E-mail: nicolas.jaouen@synchrotron-soleil.fr

Received 19 October 2007
Published 8 February 2008
Online at stacks.iop.org/JPhysCM/20/095005

Abstract

Studies of the Ag induced magnetic moments at the interfaces in an $[Ni_{81}Fe_{19}(29\ Å)/Ag(11\ Å)]_{135}$ multilayer by x-ray magnetic circular dichroism (XMCD) and x-ray resonant magnetic scattering (XRMS) at the Ag $L_{2,3}$ edges are reported. This allows us to quantify the interfacial magnetic moments as well as the extension through the silver layer. From the experimental XMCD spectra and thanks to the use of full relativistic band structure calculations, we succeed in extracting quantitative spin and orbital magnetic moments held by the 4d states of silver. Moreover, we show that, although silver has an almost full 4d band, magneto-optical sum rules can be safely applied in the case of the noble metal L edges. We find from XMCD that Ag is polarized by $Ni_{81}Fe_{19}$ and has a total magnetic moment of 0.0136 μ_B spatially averaged over the 11 Å layer thickness. XRMS analysis indicates that this induced polarization is enhanced at the interface but remains present inside the whole Ag layer, demonstrating the existence of an indirect coupling between the NiFe layers through the non-magnetic spacer.

(Some figures in this article are in colour only in the electronic version)

1. Introduction

Multilayers composed alternatively of ferromagnetic (F) and non-magnetic (NM) or antiferromagnetic (AF) films play an important role in a number of applications, such as spin-valve, magnetoresistive devices and tunnel junctions [1–3]. The insertion of an NM metallic layer between the magnetic ones may yield new magnetic properties, for example increase the anisotropy, or modify the exchange coupling between the different layers. The influence of such a layer is strongly related to the structural and magnetic order at the F(AF)/NM interface. In the case of transition metals the hybridization of the d orbitals at the interface is assumed to be the dominant effect. In particular, the magnetic polarization of the NM metallic atoms acts as a mediator of the magnetic coupling between the adjacent F(AF) layers and therefore is a key issue in the understanding of the giant magnetoresistance properties [4] in superlattices or the enhancement of the Kerr rotation [5, 6].

NiFe/Ag multilayers are to some extent well known for exhibiting a low field giant magnetoresistance (GMR) effect of the order of 5%–6% in a saturation field of a few tens of Oersted at room temperature [7, 8]. Moreover, in this magnetoresistive device it has been shown that the magnetic properties strongly depend on the thickness of the non-magnetic silver layer [9]. Another reason to study this system is that from spin-polarized photoemission experiments [10, 11] magnetic interface states showing discrete binding energies depending on the number of silver layers deposited on an iron surface have been observed. Finally, the last argument in favour of this system is the immiscibility of silver and nickel [12], leading to *a priori* sharp interdiffusion at interfaces.

In this paper we will show that, although silver has a full d shell in its atomic form, Ag atoms gave an induced moment. Our objectives were to quantify the amplitude of this moment as well as its spatial distribution through the layer thanks to the use of XMCD and XRMS [13–16] tools to extract

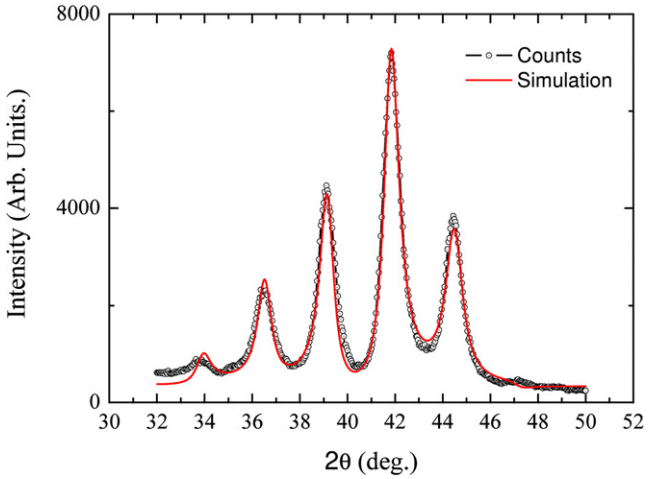

Figure 1. X-ray diffraction (black) measured with Cu Kα source (1.54 Å) together with simulation (red) (see the text for details).

inestimable information on the magnetic structure at interface in metallic thin films. The detailed structural analysis of this real multilayer device by means of x-ray diffraction and x-ray anomalous reflectivity will be the object of the first part. In the next section, we will focus on the determination of the silver induced magnetic properties from x-ray magnetic circular dichroism experiment performed at the Ag $L_{2,3}$ edges. The average Ag spin and orbital magnetic moments were obtained by the combined use of simple sum rules analysis and relativistic band structure calculation. Then, we focused on the investigation of the 4d Ag induced magnetic depth profile by means of XRMS. The induced Ag magnetic moment distribution with respect to the interface will be presented and the validity of the extracted magnetic distribution will be discussed.

2. Structural analysis

2.1. Sample preparation

The sample was prepared by dc sputtering by alternate deposition of Ag and $Ni_{81}Fe_{19}$ stoichiometric alloy on silicon substrates. The samples were grown with deposition rates of 0.98 Å s^{-1} for Ag and 0.85 Å s^{-1} for NiFe, the thickness of every layer being monitored by a quartz oscillator. A total number of 135 repetitions were achieved. More details on the sample growth can be found elsewhere [19].

2.2. X-ray diffraction

X-ray diffraction experiments have been carried out on a conventional rotating anode using the Cu Kα1 and a proportional counter. The experiment is performed in symmetrical reflection geometry at ambient temperature. The experimental XRD spectra shown in figure 1 present a series of sharp peaks arising from the artificial periodicity Λ and the corresponding average interplanar distance $\bar{d}$. The presence of several satellites surrounding the average fcc (111) multilayer Bragg peak denotes the high quality of this superlattice.

Table 1. Summarized parameters issued from the refinement of the high angle XRD pattern.

Parameter	NiFe/Ag
Multilayer period, Λ (Å)	35.49 ± 0.01
Continuous disorder, c (Å)	0.198
Nb of Ag lattice planes, $n_{Ag} \pm \Delta n_{Ag}$	5.0 ± 0.1
Nb of NiFe lattice planes, $n_{NiFe} \pm \Delta n_{NiFe}$	11.4 ± 0.3
Ag fcc (111) lattice spacing, d_{Ag} (Å)	2.367 ± 0.03
NiFe fcc (111) lattice spacing, d_{NiFe} (Å)	2.0695 ± 0.02
Average lattice spacing, $\bar{d}$ (Å)	2.16

The experimental spectrum is analysed using the superlattice refinement (SUPREX) program [20]. From the main peak positions $\bar{d}$ and Λ can be determined directly. The fitting algorithm was used to fit the entire XRD pattern, i.e. peak positions, relative intensities and line profiles. For every layer three atomic planes are allowed to expand or contract by an amount of Δd_1 and Δd_2 on the bottom and top of the layer using a linear profile [20, 21] in order to take into account the accommodation of the lattice parameter at the interface due to the NiFe and Ag lattice mismatch. The simulation was convoluted using a Lorentz function in order to account for the instrumental resolution. During the refinement process great attention has been taken for using the smallest possible number of free parameters. The solid line in figure 1 represent the best model achieved in our analysis and the corresponding parameters are given in table 1. Both the lattice spacings of Ag and NiFe are slightly enhanced by 1.5% and 1% with respect to their respective bulk values of 2.359 Å and 2.048 Å. To summarize, an overall good agreement between the experimental and calculated XRD patterns is obtained, insuring the high quality of the multilayer growth.

2.3. X-ray reflectivity

X-ray specular reflectivity (XRR) scans were measured in order to determine the parameters necessary to the analysis of the XRMS: period, individual layer thickness and interfacial roughness. The XRR measurement were recorded for several x-ray wavelengths close to the Ag L edges. The UHV reflectometer [22] available on the ID12 beamline [23] of the ESRF storage ring has been used for this purpose to avoid the strong absorption by air occurring at the energy range of interest: 3.2–3.6 keV. Figure 2 shows measured and simulated $\theta/2\theta$ scans. Regarding the small multilayer period, only three multilayer peaks were accessible in the low angular range ($\theta \leqslant 10°$).

The reflectivity spectra were refined using home-developed software [24] dedicated to XRMS analysis. The relative densities of Ag and $Ni_{81}Fe_{19}$, affecting the refractive index, were imposed to be equal to their bulk value, in agreement with XRD analysis. However, the density of the top $Ni_{81}Fe_{19}$/Ag layer has been refined to account for the expected oxidation of the sample surface and was found to be 20% lower than the bulk value. The obtained multilayer period Λ is in good agreement with the value obtained by XRD (see table 2).

The microscopic structure of the $Ni_{81}Fe_{19}$/Ag multilayer has been investigated by x-ray scattering. Although XRD

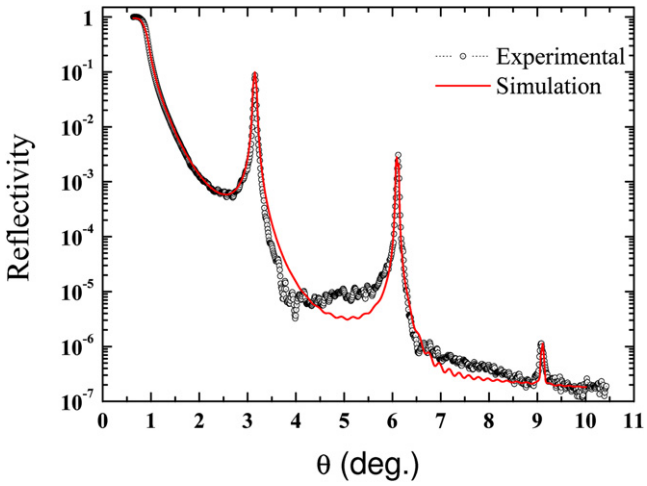

Figure 2. X-ray reflectivity (black) measured at 3340.4 eV close to the Ag L_3 resonance. Simulation (red) (see the text for details).

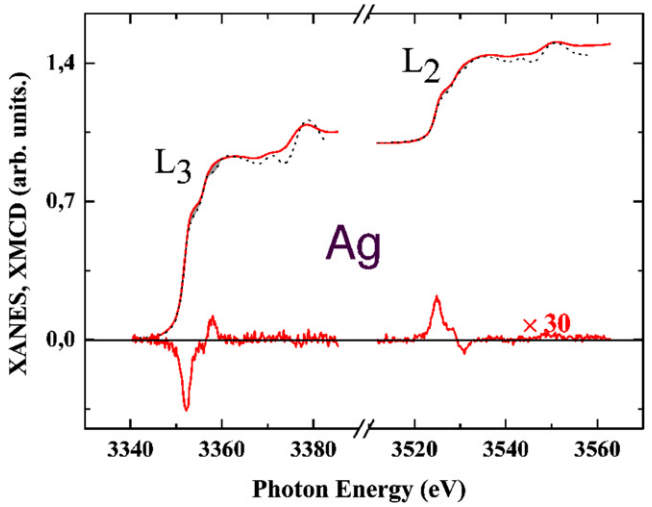

Figure 3. XAS and XMCD recorded at the Ag $L_{2,3}$ edge for the NiFe/Ag multilayer (full line) and bulk Ag (dots).

Table 2. Structural parameters issuing from the analysis of x-ray reflectivity.

Parameter	NiFe/Ag (3340.4 eV)
Multilayer period, Λ (Å)	35.36 ± 0.05
Thickness of Ag layer (Å)	11.8 ± 0.4
Thickness of NiFe layer (Å)	23.5 ± 0.4
Roughness at the NiFe/Ag interface (Å)	4.4 ± 0.2
Roughness at the Ag/NiFe interface (Å)	4.1 ± 0.2

indicates high crystalline quality and very small interfacial distortions, x-ray reflectivity shows the existence of a relatively important roughness at interfaces. At this stage, it is important to remind the reader that in specular reflectivity it is not possible to distinguish between interdiffusion and real roughness. This lets us confidently conclude that the intermixing at the interface is rather small (less than one atomic plane) but that the interfaces display correlated roughness, in close agreement with TEM and x-ray structural analysis of similar samples [25].

The structural study allows us to extract a set of parameters which reproduce separately the XRR and XRD scans. To resume, these parameters will be *in extenso* used as a fixed input for the determination of the magnetic structure of the Ag 4d induced magnetic moment.

3. Ag induced magnetism

3.1. X-ray magnetic circular dichroism: an average point of view

3.1.1. Experimental results. The magnetic properties of 4d and 5d based multilayers [6] are strongly related to the magnetic properties (i.e. amplitude, depth extension, ...) of the NM elements. XMCD is one of the most suitable techniques to obtain the average value of the spin and orbital magnetic moment of a non-full shell of a particular element. Up to now only very few experimental studies of the induced magnetic moments of 4d transition metals in thin films have been reported [26–28], and recording clear magnetic signals from noble metals at interfaces remains a challenge. This is attributed to the very small induced magnetic moments expected for noble metals. Indeed, in atomic form Ag has completely filled 4d states, implying that there is no net magnetic moment. In metallic form, there is a small number of d holes in the 4d band of Ag due to hybridization effects. Proximity with 3d ferromagnets at interfaces should then result in exchange spin polarization of Ag and the appearance of a finite induced magnetic moment. Nevertheless, related to the small number of holes, the Ag total induced magnetic moment at the Fe/Ag interface is expected from theoretical prediction to be about 0.03 μ_B [29].

With the aim to measure this magnetic polarization, Ag $L_{2,3}$ XMCD experiments have been performed at the ESRF-ID12 beamline [23]. A high magnetic field of 5 T was applied perpendicular to the sample surface and along the x-ray beam propagation to ensure complete magnetic saturation. XAS at the Ag L edges was measured in total fluorescence yield mode using circularly polarized light provided by an Helios-2 type helical undulator HU52. After the monochromator, equipped with a pair of Si(111) crystals, the polarization rate was nearly 24% and 36% at the Ag L_3 and L_2 edges respectively. XMCD spectra have been obtained as the difference of two consecutive scans for opposite polarizations of incident photons. To make sure that they were free from any artefacts the experiment was repeated with the opposite direction of the applied magnetic field. Ag $L_{2,3}$ x-ray absorption and XMCD spectra, corrected for incomplete circular polarization, are reproduced in figure 3. This represents the first, to our knowledge, XMCD spectra detected at the Ag L edges. It clearly demonstrated that the 4d electrons of Ag are polarized and carried a net induced moment ferromagnetically coupled with the NiFe layers. The Ag XANES are shown together with bulk Ag spectra taken from [30]. This comparison allows us to highlight some differences which are underlined by arrows, indicating that in this multilayer system a charge transfer occurs from Ag bands

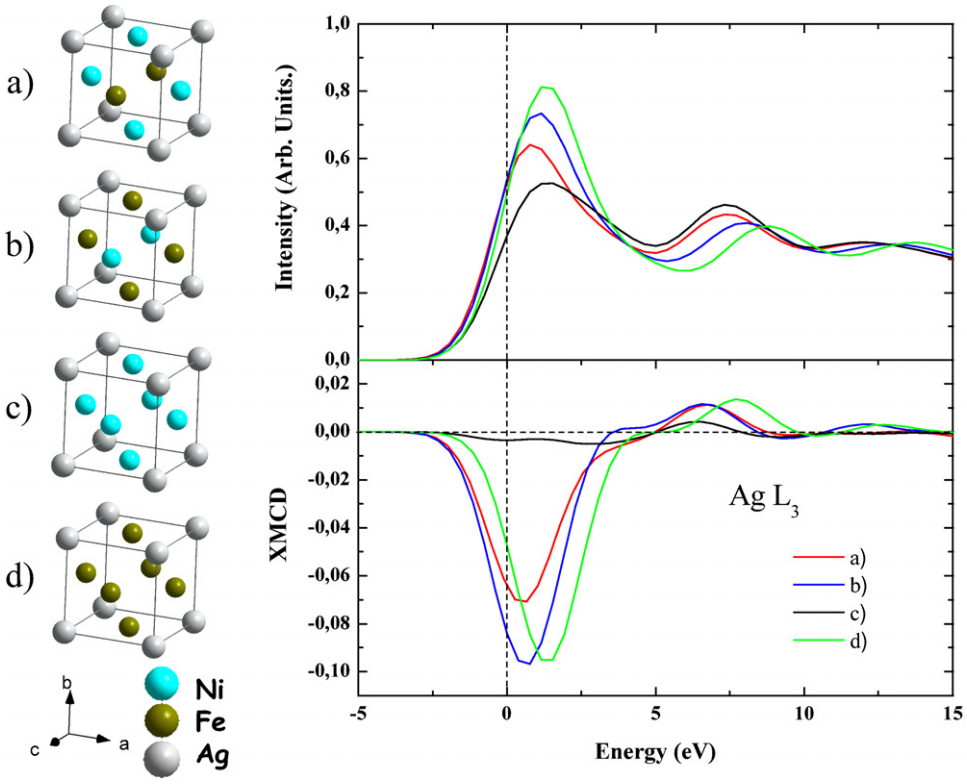

Figure 4. Absorption (top) and XMCD (bottom) spectra calculated at the Ag L_3 edge for the four fcc alloys schematically represented on the left side. For clarity only the L_3 edge is shown, but the same results apply to the L_2 one.

to the $Ni_{81}Fe_{19}$ one, leading to an increased number of holes in the Ag d states as expected.

The silver XMCD spectral shape is even more interesting because it differs strongly from the 'Lorentzian' shape usually published in the literature for other heavy 4d or 5d transition metals [6, 26]. At this stage it should be mentioned that our Ag XMCD spectra look very similar to those published for the Ge L edge, in the Fe/Ge multilayer, which also has an almost full d band [31]. The authors of [31] assigned the low energy feature to s states and the high one to d states, and assuming that the probability ratio for s versus d excitations is close to one they derived the respective signs of the Fe and Ge magnetic moments at the Fe/Ge interface. Band structure calculation was used in order to understand the electronic character of the unoccupied states contributing to the Ag XMCD signal and to check if their interpretation is also valid for silver.

3.1.2. Simulation and data analysis. The purpose of this section is not to supply a detailed theoretical investigation of the Ag induced magnetic polarization but more to understand, using the local spin density approximation linearized muffin-tin-orbital (LSDA-LMTO) method [33], the experimental XMCD spectral shape. In this sense we choose to restrict our simulations for four different but representative alloys: $NiFe_2Ag$, Ni_2FeAg, Fe_3Ag and Ni_3Ag. As the structure of $Ni_{81}Fe_{19}$ is fcc as well as Ni atoms being in majority in the multilayer, we choose to model the alloys using an fcc cubic cell and lattice parameter equal to 3.58 Å. The different alloys have been represented in the left part of figure 4. We would like to point out that no attempt was made to adjust any parameters.

The top of figure 4 displays the Ag L_3 x-ray absorption spectrum calculated in the dipolar approximation, without continuum, for the $NiFe_2Ag$, Ni_2FeAg, Fe_3Ag and Ni_3Ag models. The simulations were convoluted by a Lorentzian function of 1.5 eV to account for both the experimental resolution (0.3 eV for Si(111)) and the core–hole effects (1.2 eV) [32]. It should be noted that the 'white-line' intensity increases with the number of Fe nearest neighbours. It confirms that a significant charge transfer with Fe neighbours occurs. However, the presence of Ni atoms is also important, because it appears to be responsible for the shift towards low energy of the second feature (located at ≈7 eV) together with a small shift toward high energy of the first feature (≈2 eV).

The bottom part of figure 4 displays the corresponding Ag L_3-edge XMCD spectra. Clearly an important change in amplitude and shape occurs between the FeAg, Ni_2FeAg models on one hand and Ni_3Ag on the other hand. The important negative peaks at low energy disappear when replacing Fe by Ni atoms, although the positive high energy is only slightly reduced. If we now turn to compare the Ni_2FeAg and the Fe_3Ag one, the calculated XMCD signal decreases when the number of Fe neighbours is reduced. Interestingly, the introduction of a ratio of two Ni for one Fe atom leads to a small shift towards low energy of the whole XMCD spectrum as well as an increase of the overlap between the negative and positive peaks. In view of these results, we have demonstrated that the Ag L edge XAS and XMCD spectra are

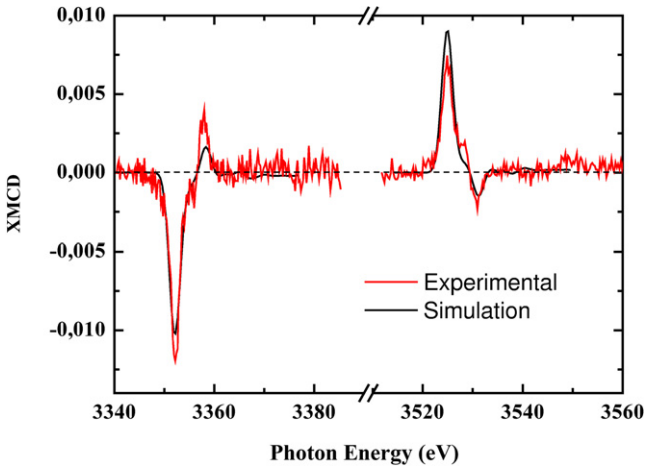

Figure 5. Ag $L_{2,3}$ experimental and calculated XMCD spectra for the Ni_2FeAg alloy model. The simulated spectra have been divided by a scaling factor for clarity (see the text for details).

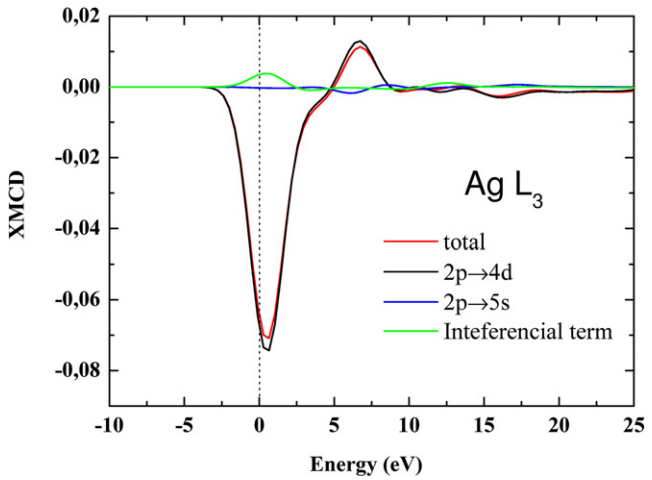

Figure 6. Theoretical XMCD spectra (red) compared with the respective contribution of the two allowed dipolar transitions p → d (black) and p → s (blue). In green is the term of interference between the two channels.

strongly dominated by the presence of Fe neighbours through the charge transfer process. But we have also shown that Ni atoms influence the position in energy of the relative features through modification of the density of states at the Fermi level.

The comparison between the experimental Ag $L_{2,3}$ XMCD and the one obtained for the Ni_2FeAg alloy are represented in figure 5. As expected the calculated amplitude does not match the experimental one at all, but when divided by a scaling factor of 7.2 it appears clearly that all the spectroscopic features are very well reproduced. Although our intention is certainly not to argue that a model of an interface in a multilayer by an alloy cell is rigorous or even correct, the good agreement can be explained as follows: as we make sure that the mean Ag to first neighbour distance in our simulations are taken as close as possible to the probed sample, the dominant effect will be charge transfer through 3d–4d hybridization over structural effects. To go further, we look at the respective weight of the p → d transition versus the p → s one. For comparison figure 6 displays the respective contributions of these two allowed dipolar transitions together with the simulation already discussed above. These two virtual XMCD spectra have been obtained by switching on and off in the calculation each transition respectively. From our calculation, we found that, contrary to what has been claimed for the Fe/Ge system [31], in the NiFe/Ag case the p → s dipole channel is one order of magnitude smaller than the p → d, mainly due to transition matrix element effects. It is also interesting to note that the p → s is even smaller than the interference between the two allowed channels (see figure 6). Thus, our calculations confirm that the Ag $L_{2,3}$-edge XANES is clearly dominated by the p → d channel as already published by Drude *et al* [34], but in addition reveals the relative contribution of both dipolar channels in the XMCD spectra of silver L edges.

3.1.3. Application of sum rules in the case of silver L edges. In this section we would like to discuss the application of the magneto-optical sum rules in the particular case of Ag $L_{2,3}$ XMCD spectra. In the previous section, we demonstrated that at the Ag L edges the contribution due to the p → d dipole channel occupies a dominant part of the total dichroism and successfully explained the existence of the two main peaks in the Ag spectra. We are therefore led to the conclusion that the magneto-optical sum rules [17, 18] can be safely applied at the Ag $L_{2,3}$ edges in order to derive the magnetic moment of silver.

Table 3. Calculated 4d spin and orbital magnetic moments of silver for the different alloys.

Parameter	Fe_3Ag	Ni_3Ag	Ni_2FeAg	$NiFe_2Ag$
m_S (μ_B/atom)	0.139	0.0097	0.095	0.137
m_L (μ_B/atom)	0.005	0.0005	0.003	0.009
m_{tot} (μ_B/atom)	0.144	0.0102	0.098	0.146

Prior to this experimental determination, we summarize the calculated Ag magnetic moments of the different alloys used (see table 3). Using the values obtained for Ni_2FeAg and applying the scaling factors already used in figure 5, we can estimate the spin and orbital magnetic moments held by silver in the probe sample. The estimation gives a value of 0.0132 μ_B/atom for the spin moment and 0.0004 μ_B/atom for the orbital magnetic moment.

The electron expectation values of the orbital moment and spin moment are related by the sum rules to the integrated XMCD signal [17, 18]. Only considering the p → d transition, the principal unknown is the total number of holes h_T in the d band of silver, although they could be estimated from band model calculation. Nevertheless, to determine properly h_T the simple approach using an alloy is certainly not valid, and one needs to construct a multilayer super-cell accounting for the presence of the NiFe alloy, which is far beyond the scope of our paper.

For this purpose, we refer to the spirit of the qualitative approach developed in [35, 36] for Pt and applied more recently to silver in Ag–Au alloy [37, 34]. This allows us to

express the integrated absorption coefficient near L_2 and L_3 as

$$A_{L2} = C(R_d^{2p_{1/2}})^2 \frac{h_{3/2}}{3}$$

$$A_{L3} = C(R_d^{2p_{3/2}})^2 \frac{6h_{5/2} + h_{3/2}}{15}$$

where C is a numerical constant [36] which depends on the element whose edge is probed, but in any chemical state of this element. R_d^{nlj} are the radial parts of the dipole transition matrix element connecting the core state (n, l, j) with the d states and h_j is the number of holes characterized by total angular momentum quantum number J. Before we continue further, it seems important to recall the hypothesis behind this approach and at the same time that it is fully compatible with the one behind the magneto-optical sum rules [17, 18]: the differences between $R_{d_{5/2}}(r, E)$ and $R_{d_{3/2}}(r, E)$ as well as their slight energy dependence over the width of the d band are neglected. Moreover, the transition from the core level to the 5s band final states is also neglected, but this can be done safely in our system as demonstrated in the previous section.

By solving this equation system and taking into account that the branching ratio differs slightly from the statistical value of 2, due to difference in the radial part of the dipole matrix element, but is closer to 2.17 [38] for the silver $L_{2,3}$, the equation above can be reformulated:

$$h_t = 2.25(A_{L3} + 1.085A_{L2})/(C\ R_d^{2p_{1/2}}).$$

Usually, one can determine properly the areas A_{L3} and A_{L2} by subtracting from the experimental XANES the contribution from all other electrons in the systems. Typically two types of approximations are used: (i) assume that this contribution has an arctangent shape (ii) or subtract an appropriate L edge of another element which has no significant structure, i.e. L edge of Au and Ag for 5d and 4d elements. In the case of silver, it is meaningless to use the first approximation and difficult to neglect the 'white-line' area of the bulk silver as illustrated in figure 3.

In order to avoid the difficulties in determining the numerical value of $R_d^{2p_{1/2}}$ by accurate band structure calculation for a multilayer super-cell, we choose to follow the method explicitly describe in [39], which is to not intended to find the total number of holes but instead to determine the fractional change in the number of holes relative to a reference material. In our case the reference will be the Ag bulk spectrum displayed in figure 3. Adopting the notation of Mansour *et al* [39], the total number of holes of the probe sample h_{Ts} can be expressed as a function of the number of holes h_{Tr} of the reference material:

$$h_{Ts} = (1.0 + f_d)h_{Tr}$$

where f_d depends uniquely on the grey area in the XANES spectra in figure 3 and on the combined area for the reference compounds $A_{3r} + 1.085A_{2r}$, which is a constant for each type of element. This last factor can be determined [36] by assuming that the ratio $(h_{5/2})/(h_{3/2})$ is known for the reference material. From our computed estimation we found for pure silver a value of 1.66 for this ratio (close to the statistical ratio of 1.5) and a total number of d holes of 0.359 (in good agreement with the early reported theoretical estimation of 0.349 [40]). The relative 'white-line' intensities $\Delta A_{3,2}$ were obtained by subtracting a reference Ag spectrum taken from [30] and $A_{3r} + 1.085A_{2r}$ have been extracted from the same reference Ag spectra. Following the approach described in [35, 39], a value of 0.22 has been obtained for f_d corresponding to a total number of holes of ≈0.437 in our multilayer sample.

Having determined h_{Ts}, the magnetic moment of Ag can be estimated and separated into spin and orbital contributions by applying the so-called 'sum rules' [18, 17]. Our analysis provides for the total magnetic moment of Ag the value $\mu_{tot} = 0.0135\ \mu_B$/atom, whereas the orbital magnetic moment is found to be very small, $\mu_L = 0.001\ \mu_B$/atom. At this point one has to recall that XMCD probes the average Ag magnetic moment in the sample and due to possible non-uniformity through the Ag layer this value is difficult to interpret. With the intention to be more quantitative in the determination of the Ag induced magnetic moment at the NiFe interface, the determination of this extension through the layer will be the subject of the next section.

3.2. X-ray resonant magnetic reflectivity: a depth resolved point of view

3.2.1. Basics. X-ray resonant magnetic scattering is highly sensitive to the distribution of magnetization of the resonant atom. At the Ag L resonance, transitions from the 2p core level to the small unoccupied part of the 4d band are excited, in the same way as for absorption, and the corresponding magnetic reflectivity experiment will probe the magnetic structure related to these 4d electrons under some assumptions which will be discussed in the next paragraph. Unfortunately, the total resonant reflectivity is a mixing of both magnetic and charge responses. In order to be more sensitive to the magnetic structure, especially when the latter is expected to be small, it is more convenient to extract a difference signal by reversing either the direction of the applied magnetic field or the helicity of the incoming beam.

We analyse quantitatively the measured magnetic reflectivity signal with the magneto-optical formalism, which can be considered as an alternative of the distorted-wave Born approximation which has been recently developed [42, 43]. In the so-called transverse magneto-optical Kerr (TMOKE) geometry, i.e. external field applied in the sample plane and perpendicular to the diffraction plane, it is relatively easy to solve Maxwell's equation due to the decoupling of the magnetic and dielectric terms [44]. Unfortunately, such a simple approach fails for the more convenient geometry (LMOKE) in the medium to hard x-ray range (where all the reflectivity pattern is concentrated in the low angle region), i.e. when one uses circularly polarized x-rays with magnetic field applied along the beam direction. Although recent work prefers a pure numerical resolution [45], we choose to develop, in first order of the magnetic contribution, the Maxwell equation [24], extending the approach of Zak *et al* [46] by taking into account interfacial roughness following the theory of Vidal and Vincent [47]. This approach has

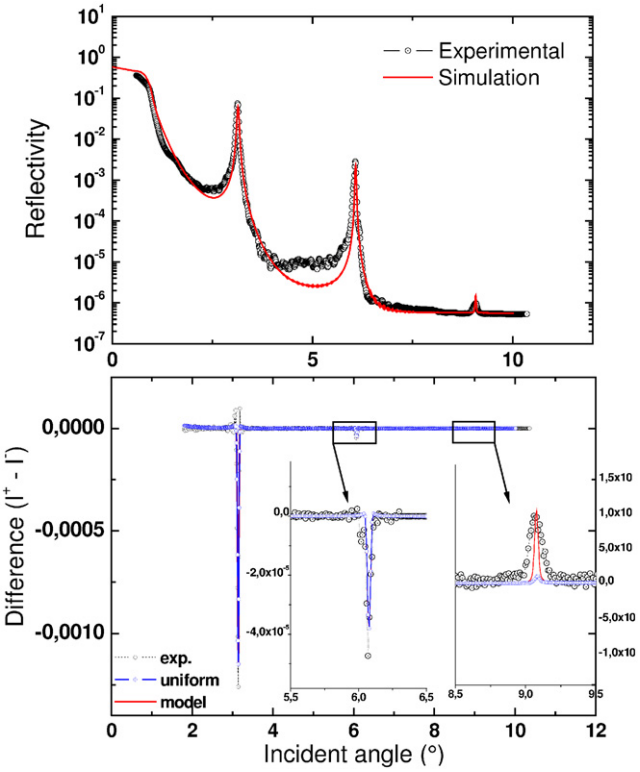

Figure 7. X-ray resonant magnetic reflectivity results. Angular dependence of the magnetic reflectivity measured at 3352.5 eV close to the Ag L_3 edge: experimental (dark line) and calculated curves (red and blue lines) using the magnetic profile represented at the bottom of the same figure.

been proved to work in soft x-rays [48, 24] and is expected to be also valid at higher energies.

The use of an optical approach accounting for absorption and interfacial roughness will be shown to be extremely important for the conclusion arising from XRMS, at least when interference effects become significant. This was clearly the case for the studied multilayer, which presents a high number of repetitions at medium x-ray energies where the attenuation length does not exceed the total sample thickness. This optical approach can be considered as an alternative to the use of a strict dynamical theory of x-ray scattering.

3.2.2. Results. XRMS experiments were also carried out at the ESRF beamline ID12 described in [23, 49]. XRMS was measured using the UHV-compatible reflectometer [14]. The XRMS curves were recorded at room temperature and an applied magnetic field of 0.4 T in the geometry of the longitudinal magneto-optical Kerr effect as described in the previous section. This field was high enough to saturate the ferromagnetic layers. Figure 7 displays the x-ray reflectivity as a function of the incident angle (top) and the corresponding magnetic contribution (bottom) at the Ag L_3 edge. This magnetic signal is defined as $(I^+–I^-)$, where $I^{+(-)}$ are the diffracted intensities of circularly polarized x-rays for magnetization of the sample being parallel (antiparallel) to the photon propagation direction. In order to avoid any experimental artefacts, the XRMS curves were also recorded by reversing the helicity of the x-rays emitted by a Helios2 helical undulator [23]. Due to the rather low energy of the Ag L_3 edge (3352.5 eV) only three superlattice Bragg peaks have been experimentally accessible. It is important to note that due to the rather huge absorption effect expected at this intermediate energy range and the very strong amplitude of the first multilayer Bragg peak, shown at the top of figure 7, the use of the kinematical approach is no longer valid. As already mentioned, we used the structural parameters from our structural study (section 2) to model XRMS spectra.

The introduction of roughness effects leads to good agreements with the experimental data and allows us to obtain the induced Ag magnetization profile as displayed by the straight lines in the same picture. The Ag layer is described by only three effective sublayers in regard to the small number of measured low angle Bragg peaks. The two interfacial ones have an individual thickness corresponding to the (111) Ag interplanar distance of 3 Å. To avoid too many parameters, the central part of the stack is kept as one Ag layer of 5.8 Å. Before starting any refinement procedure, we simulate XRMS spectra for a uniform magnetic distribution over the whole Ag layer. The result is displayed as a blue line in figure 7 and a clear disagreement between the experimental and calculated magnetic signals can be seen at the third Bragg peaks. To go further, we perform simulation using several arbitrary models of the Ag magnetic distribution, leading to the conclusion that the third Bragg peak is strongly dependent on the magnetization profile. A refinement of the three amplitudes allows us to reproduce quite well the experimental spectrum and indicates also that the amplitude decreases on going away from the NiFe/Ag interface. Keeping in mind the inherent limitation of this approach as already stressed in detail in our previous publications [13, 14], the quantitative amplitude of the silver magnetic moment has been derived. In addition it is important to recall, as pointed out recently [41], that the basic assumption thereby is that the magnetic contributions to the optical constants of the various layers are proportional to the magnetic moments of these layers. They demonstrate using *ab initio* calculations that this assumption is approximatively valid at the Pt L edges for a Co–Pt multilayer system. They recall that the assumption is approximatively valid mainly if the spin–orbit coupling is not too strong [41]. Considering that the silver spin–orbit coupling of Ag is much smaller than for Pt, we regard this assumption as valid for our purpose. Absolute values of magnetic moments per Ag atom were obtained using the XMCD results as reference and we found an Ag total magnetic moment of 0.0147 μ_B/atom at the interface and a slightly reduced moment of 0.0125 μ_B/atom in the central thicker slab. The results of this analysis show that the interface atoms are strongly polarized at a distance of up to three atomic planes from the interface. We explain the apparent disagreement with results from photoemission [10, 11] by the lack of sensitivity to the smallest magnetic moment held by the Ag atoms in the central slabs. However, our results are in good agreement with the results obtained concerning heavy transition metal elements, either 4d [26] or 5d [6, 50, 51].

4. Summary

Using an element-specific probe, the magnetic properties of silver layers of a NiFe/Ag multilayer were studied. Structural modelization of the sample under study was obtained from XRD and XRR techniques. The high quality of the XMCD data allowed us to analyse the spectral shape in detail using modern band structure calculations. This combination of experimental and theoretical results allowed us to obtain information about the electronic structure and magnetic properties of Ag in an NiFe/Ag multilayer. Quantitative estimation of the Ag magnetic moment averaged over the silver layer has been reported for the first time. Finally, spatially resolved magnetization profiles were obtained from fits of XRMS data using an optical theory calculation of the magnetic contribution in the reflectivity spectrum. We found that the Ag atoms are still magnetically polarized up to three atomic planes from the interfaces. We would like to conclude by pointing out that the noble metal is not only polarized strictly at the interface by direct Fe–Ag hybridization but, despite the small number of holes in the d band, the Ag–Ag interactions permit us to polarize the adjacent atomic planes throughout the 11.84 Å Ag layer.

Finally, we have also shown that the magneto-optical sum rules [17, 18] can be safely applied at the $L_{2,3}$ edges of noble metals, offering an unique possibility to selectively extract their spin and orbital magnetic moments from x-ray magnetic circular dichroism measurement.

References

[1] Nogueś J and Schuller I K 1999 *J. Magn. Magn. Mater.* **192** 203
[2] Berkowitz A E and Takano K 1999 *J. Magn. Magn. Mater.* **200** 552
[3] Stiles M D and McMichael R D 1999 *Phys. Rev.* B **59** 3722
[4] Baibich M N, Proto J M, Fert A, Nguyen Van Dau F, Petroff F, Eitienne P, Creuzet G, Friederich A and Chazelas J 1988 *Phys. Rev. Lett.* **61** 2472
[5] Bennet W R, Schwarzacher W and Egelhoff W F Jr 1990 *Phys. Rev. Lett.* **65** 3169
[6] Wilhelm F, Angelakeris M, Jaouen N, Poulopoulos P, Papaioannou E T H, Mueller Ch, Fumagalli P, Rogalev A and Flevaris N K 2004 *Phys. Rev.* B **69** 220404(R)
[7] Hylton T L, Coffey K R, Parker M A and Howard J K 1994 *J. Appl. Phys.* **75** 7058
[8] Christides C, Stavroyiannis S and Niarchos D 1996 *J. Appl. Phys.* **80** 4512
[9] Gan'shina E, Guschin V, Kirov S, Perov N, Syr'ev N and Brouers F 1997 *J. Magn. Magn. Mater.* **165** 346
[10] Brookes N B, Chang Y and Johnson P D 1991 *Phys. Rev. Lett.* **67** 354
[11] Smith N V, Brookes N B, Chang Y and Johnson P D 1994 *Phys. Rev.* B **49** 332
[12] Massalki T B, Murray J L, Bennett L H and Bakr H (ed) 1986 *Binary Alloy Phase Diagrams* (Metals Park, OH: American Society for Metals)
[13] Sève L *et al* 1999 *Phys. Rev.* B **60** 9662
[14] Jaouen N *et al* 2002 *Phys. Rev.* B **66** 134420
[15] Ishimatsu N, Hashizume H, Hamada S, Hosoito N, Nelson C S, Venkataraman C T, Srajer G and Lang J C 1999 *Phys. Rev.* B **60** 9596
[16] Jaouen N, van der Laan G, Johal T K, Wilhelm F, Rogalev A, Mylonas S and Ortega L 2004 *Phys. Rev.* B **70** 094417
[17] Thole B T, Carra P, Sette F and van der Laan G 1992 *Phys. Rev. Lett.* **61** 1943
[18] Carra P, Thole B T, Altarelli M and Wang X-D 1993 *Phys. Rev. Lett.* **70** 694
[19] Rodmacq B, Hillairet J, Laugier J and Chamberod A 1990 *J. Phys.: Condens. Matter* **2** 95
[20] Fullerton E E, Schuller I K, Vanderstraeten H and Bruynseraede Y 1992 *Phys. Rev.* B **45** 9292
[21] Fullerton E E, Schuller I K, Vanderstraeten H and Bruynseraede Y 1993 *Phys. Rev.* B **45** 9292
[22] Jaouen N, Wilhelm F, Rogalev A, Goulon J and Tonnerre J M 2004 *AIP Conf. Proc.* **705** 1134
[23] Goulon J, Rogalev A, Gauthier C, Goulon-Ginet C, Paste S, Signorato R, Neumann C, Varga L and Malgrange C 1998 *J. Synchrotron Radiat.* **5** 232
[24] Jaouen N 2001 *PhD Thesis* Grenoble
[25] Chládek M, Dorner C, Matner M, Hoffmann H and Valvoda V 1997 *J. Phys.: Condens. Matter* **9** 4557
[26] Vogel J, Fontaine A, Cros V, Petroff F, Kappler J-P, Krill G, Rogalev A and Goulon J 1997 *Phys. Rev.* B **55** 3663
[27] Chaboy J, Bartolomé F, Ibarra M R, Marquina C I, Algarabel P A, Rogalev A and Neumman C 1999 *Phys. Rev.* B **59** 3306
[28] Hashizume H, Ishiji K, Lang J C, Haskel D, Srajer G, Minaŕ J and Hebert H 2006 *Phys. Rev.* B **73** 224416
[29] Tyer R, van der Laan G, Temmerman W M, Szotek Z and Hebert H 2003 *Phys. Rev.* B **67** 104409
[30] Kolobov A V, Rogalev A, Wilhelm F, Jaouen N, Shima T and Tominaga T 2004 *Appl. Phys. Lett.* **84** 1641
[31] Freeland J W, Kodama R H, Vedpathak M, Erwin S C, Keavney D J, Winarski R, Ryan P and Rosenberg R A 2004 *Phys. Rev.* B **70** 033201
[32] Sipr O, Rocca F and Dalba G 1999 *J. Synchrotron Radiat.* **6** 770
[33] Antonov V, Harmon B and Yaresko A 2004 *Electronic Structure and Magneto-Optical Properties of Solids* (Dordrecht: Kluwer)
[34] Drude W, Treusch R, Sham T K, Bzowski A and Soldatov A V 1998 *Phys. Rev.* B **58** 6871
[35] Brown M, Peierls R E and Stern E A 1977 *Phys. Rev.* B **15** 638
[36] Mattheiss L F and Dietz R E 1980 *Phys. Rev.* B **22** 1663
[37] Bzowski A, Sham T K and Yiu Y M 1994 *Phys. Rev.* B **49** 13776
[38] Chantler C T 1995 *J. Phys. Chem. Ref. Data* **24** 71
[39] Mansour A N, Cook J W Jr and Sayers D E 1984 *J. Phys. Chem.* **88** 2330
[40] Lu Z W, Wei S-H and Zunger A 1991 *Phys. Rev.* B **44** 10470
[41] Fähnle M, Steiauf D, Martosiswoyo L, Goering E, Brück S and Schütz G 2007 *Phys. Rev.* B **55** 144415
[42] Lee D R, Sinha S K, Haskel D, Choy Y, Lang L C, Stepanov S A and Srajer G 2003 *Phys. Rev.* B **68** 224409
[43] Choy Y, Haskel D, Camley R E, Lee D R, Lang J C, Srajer G, Liang J S and Bader S D 2004 *Phys. Rev.* B **70** 134420
[44] Zaharko O, Oppeneer P M, Grimmer H, Horisberger M, Mertins H-Ch, Abramsohn D, Schäfers F, Bill A and Braun H-B 2002 *Phys. Rev.* B **66** 134406
[45] Sacchi M and Mirone A 1998 *Phys. Rev.* B **57** 8408
[46] Zak J, Moog E R, Liu C and Bader S D 1991 *Phys. Rev.* B **43** 6423
[47] Vidal B and Vincent P 1984 *Appl. Opt.* **23** 1794
[48] Jaouen N *et al* 2001 *Appl. Phys.* A **73** 711
[49] Goulon J *et al* 2005 *J. Synchrotron Radiat.* **12** 57
[50] Wilhelm F *et al* 2000 *Phys. Rev. Lett.* **85** 413
[51] Geissler J, Goering E, Justen M, Weigang F, Schuẗz G, Langer J, Schmitz D, Maletta H and Mattheis R 2001 *Phys. Rev.* B **65** 020405(R)